# High Curie temperature perovskite $BiInO_3$–$PbTiO_3$ ceramics

Runrun Duan and Robert F. Speyer
*School of Materials Science and Engineering, Georgia Institute of Technology, Atlanta, Georgia 30332-0245*

Edward Alberta
*TRS Technologies, State College, Pennsylvania 16801*

Thomas R. Shrout
*Materials Research Laboratory, Pennsylvania State University, University Park, Pennsylvania 16802-4800*

(Received 18 February 2004: accepted 26 April 2004)

The extent of $BiInO_3$ substitution in the perovskite system $x$BiInO$_3$–$(1 - x)$PbTiO$_3$ and the corresponding raise in the Curie temperature were investigated using thermal analysis, dielectric measurements, x-ray diffraction, and electron microscopy. Maximum tetragonal perovskite distortion ($c/a = 1.082$) was obtained for $x = 0.20$, with a corresponding Curie temperature of 582 °C. Phase-pure tetragonal perovskite was obtained for $x \leqslant 0.25$. Compound formation after calcining mixed oxide powders resulted in agglomerated cube-shaped tetragonal perovskite particles, which could be fired to 94.7% of theoretical density (TD). Sol-gel fabrication resulted in nano-sized tetragonal or pseudo-cubic perovskite particles, which after two-step firing, resulted in a tetragonal perovskite microstructure at as high as ($x = 0.20$) 98.1% of TD.

## I. INTRODUCTION

Piezoelectrics of commercial interest for transducer and actuator applications are generally comprised of solid solutions of $Pb(Zr_{1-x}Ti_x)O_3$ (PZT), which lie near the rhombohedral–tetragonal phase boundary (i.e., morphotropic phase boundary, MPB).[1] Applications such as actuators for automotive fuel injectors, gyros, or vibration dampening, often require broad operational temperature ranges, which can exceed the Curie temperature of PZT.[2,3]

Goldschmidt proposed the tolerance factor

$$t = rA + rO / ; sj2 (rB + rO)$$

where $r_A$, $r_B$, and $r_O$ represent ionic radii in an $ABO_3$ perovskite-structured compound such $BaTiO_3$. The perovskite structure is expected to be stable over range $0.77 < t < 0.99$, or $0.88 < t < 1.09$, depending on the assumed coordination of the A sites.[4] Recently, a trend of increasing Curie temperature has been observed with decreasing $t$[5] for a series of $x$ABO$_3$–$(1 - x)$PbTiO$_3$ (where $x$ is mole fraction) MPB compositions, though these compositions had yet to be prepared, due to their inherent perovskite instability, resulting in excessive pyrochlore formation. $ABO_3$ constituents $BiInO_3$ and $BiYbO_3$ were projected to result in Curie temperatures of 550 and 650 °C, respectively, which is significantly higher than 386 °C for MPB $Pb(Zr_{1-x}Ti_x)O_3$.[5] The work detailed herein concentrated on fabricating perovskite-structured $x$BI–$(1 - x)$PT solid solutions devoid of non-perovskite second phases, and on seeking compositions ($x$) corresponding to the MPB.

## II. EXPERIMENTAL PROCEDURE

### A. Mixed oxide powders

Powder mixtures of $x$BI–$(1 - x)$PT, with $x$ values from 0.05 to 0.35 in steps of 0.05 were prepared by ball-milling PbO (Hammond Lead Products), $Bi_2O_3$ (Alpha Aesar), $In_2O_3$ (Alpha Aesar) and $TiO_2$ (anatase, Aldrich Chemical Co., Inc.) at room temperature in plastic jars for 4 h in ethanol and de-ionized water (1:1 ratio), using 8 mm diameter partially stabilized zirconia milling media. An additional 3 mol% PbO was added to ensure a Pb-rich atmosphere during firing. Each slurry was then dried for 12 h at 90 °C. The as-dried mixture was ground using an alumina mortar and pestle, and passed through an 80-mesh sieve.

Portions of the resulting powder were pressed at 150 MPa into cylindrical pellets (16 mm in diameter and 1.7 mm in height). These compacts were fired in covered MgO crucibles at 450, 750, 825 (all held for 4 h), 1000 and 1100 °C (both held for 2 h, the shorter time was used to reduce the PbO loss). Heating rates were 8 °C/min and

DOI: 10.1557/JMR.2004.0282

  

cooling occurred in the furnace with no power applied to the heating elements. Additional loose powder of the same composition as the pellets was placed around the pressed pellets in the crucible to create an overpressure of the volatile constituents.

Powder mixtures were also fired via a two-step process to form dense sintered compacts. Powders were shaped using a die and punch into softly pressed cylindrical disk compacts, and calcined (reacted) in magnesia crucibles at 850 °C for 4 h. These were then re-milled for 4–5 h, dried, passed through an 80-mesh sieve, and then pressed at 150 MPa into cylindrical pellets of 6.2 mm in diameter and 5 mm in height. These green bodies were then fired in covered MgO crucibles with surrounding powder of the same composition, heating at 8 °C/min to 1050, 1100, or 1150 °C and soaking for 2 h. A sample calcined at 1000 °C for 2 h was also prepared by crushing with a mortar and pestle, re-pressing at 150 MPa, and then heating at 8 °C/min to 1150 °C and soaking for 2 h.

### B. Sol-gel prepared powders

Polycrystalline samples of BI-PT compositions were prepared from lead acetate [$Pb(COOCH_3)_2$, Research Chemical Ltd.] indium acetate [$In(COOCH_3)_3$, Indium Corporation of America], bismuth acetate [$BI(COOCH_3)_3$, Alfa Asear] and titanium *n*-butoxide ($TiC_{16}H_{36}O_4$, ACROS). Glacial acetic acid, isopropyl alcohol, and distilled water were used as solvents. Lead acetate was dissolved in glacial acetic acid (650 g/l). Separately, a 1:1 molar mixture of bismuth and indium acetates was dissolved in a 1:4 volume mixture of distilled water and glacial acetic acid, so that there was 50 g indium acetate and 66.25 g bismuth acetate to 1 l solvent. This mixture was heated at 80 °C in a conical flask under stirring for 1 h. Titanium *n*-butoxide was dissolved in glacial acetic acid and isopropyl alcohol (1:1:1 in volume ratio), and this solution was poured slowly into the previous mixture under stirring to obtain a sol. Mixtures of the three solutions were of molar ratios to generate $x$ values identical to those prepared for the mixed oxides. The sol was held at 70 °C under constant stirring for 48 h to yield a light yellow gel. These gels were then dried at 100 °C for 24 h. These were in turn ground using a mortar and pestle into powders and heated at 3 °C/min to soaking temperatures of 450, 500, 550, and 600 °C for 6 h, in covered magnesia crucibles. In a two-step process, samples heat-treated at 600 °C were crushed using a mortar and pestle and then pressed (150 MPa) into cylindrical pellets 5 mm thick and 6.2 mm in diameter, and heated at 4 °C/min to 1000 or 1150 °C, soaking for 2.5 h (a 900 °C soak was also evaluated for $x = 0.15$). As before, loose powder of the same composition was placed around the pellets in the covered MgO crucibles.

### C. Characterization

Phase analyses of heat-treated and crushed (using a mortar and pestle) compositions were performed by powder x-ray diffraction (XRD) using Cu $K_\alpha$ radiation at a scanning speed of 0.015° per step with one step per second. Lattice parameters for the tetragonal perovskite-structured phase were determined using the extrapolation method,[6] in which lattice parameters, calculated from each diffraction peak, were plotted against (1/2) ($\cos^2\theta / \sin\theta + \cos^2\theta/\theta$) <*hk*0> diffraction lines were used to determine the lattice parameter *a,* and <00*l*> diffraction lines were used to determine the lattice parameter *c*. The true lattice parameters were determined by extrapolating to where this function was zero ($2\theta = 180°$).

Crystal size for sol-gel-prepared powders was calculated based on XRD line broadening for the pseudo-cubic or tetragonal perovskite (111) peak 40° 2θ using the Scherrer equation[6]

$$B = \frac{0.9\lambda}{t\ cos\ \theta}$$

where $B$ is the broadening of the diffraction peak measured as its width at half its maximum intensity, $t$ is the particle diameter, $\lambda = 0.15406$ nm and θ is the Bragg angle. $B$ was determined by the equation $B^2 = B_M{}^2 - B_S{}^2$, where $B_M$ is the measured breadth of the diffraction peak at half its maximum intensity and $B_S$ is the measured breadth at half-maximum intensity of the corresponding diffraction peaks from a coarse-grained sample of the same composition. The coarse-grained samples were those prepared through sintering of mixed oxide powders, which had average grain sizes of well over 1 μm.

Curie temperatures were identified using differential scanning calorimetry (DSC; TA Instruments DSC cell with an Innovative Thermal Systems interface), under heating rates of 8 °C/min. Reactions occurring in sol-gel prepared powders were characterized using thermogravimetric analysis (TG; Rheometric Scientific STA 1500) and differential thermal analysis (DTA; Perkin-Elmer DTA 1700).

Electrical measurements of capacitance and loss were made on selected samples with sputtered-on gold electrodes to determine the Curie temperature (for conformation of DSC results). A multi-frequency LCR meter interfaced with a computer-controlled furnace was used between ambient temperature and 650 °C. The dielectric permittivity was calculated from the capacitance using the parallel plate approximation. Only frequencies at 100 kHz and 1 MHz were used because of the relatively high losses at temperatures greater than 400 °C.

Weights and dimensions of fired pellets were measured, from which dimensional densities were calculated. Densities of more dense specimens were determined using Archimedes method. Microstructure was characterized using scanning electron microscopy [SEM; Model

S-800, Hitachi High Technologies, Tokyo, Japan, with a energy dispersive spectrometer (EDS), Thermo Noran, Middleton, WI, and Model 1530 SEM, LEO Electron Microscopy, Inc., Oberkochen, Germany] and transmission electron microscopy (TEM; model HF2000, Hitachi High Technologies, Tokyo, Japan).

## III. RESULTS

### A. Mixed oxides

Table I lists the phases identified for $x$BI–$(1 - x)$PT compositions based on comparison with the ICDD database as a function of temperature. XRD patterns for $x = 0.15$ are shown as a function of calcination temperature in Fig. 1. Batch oxides reacted between 450 and 750 °C to form a phase which can be roughly correlated to a cubic perovskite structure ("pseudo-cubic," see discussion). At and above 825 °C for $x \leqslant 0.10$, and at and above 1000 °C for $x \geqslant 0.15$, peaks corresponding solely to the tetragonal perovskite structure were detected, along with trace amounts of $In_2O_3$. For $x \geqslant 0.30$ and temperatures at and above 750 °C, the concentration of $In_2O_3$ was more substantial, and peaks corresponding to $Pb_3Bi_2O_6$ were identified, in addition to the tetragonal perovskite-structured phase.

After reaction heat treatment at or above 1000 °C, the $a$ lattice parameter of the tetragonal perovskite-structured phase dilated in roughly even steps with increasing $x$ up to $x = 0.30$, while dilation of the $c$ lattice parameter with $x$ was greater in magnitude, yet halted at $x = 0.20$ (Fig. 2). Corresponding, the $c/a$ ratio increased up to $x = 0.20$, and then decreased over the range $0.20 \leqslant x \leqslant 0.30$, showing no clear trend thereafter.

Figure 3(a) is a SEM micrograph of a pressed mixed oxide particle compact prior to heat-treatment, showing an average particle size of 200 nm, with the exception of $Bi_2O_3$ particles (as indicated by EDS), which were in the range of 5 μm. After heat treatment at 750 °C, particles similar in appearance as the 200 nm starting particles were seen, but voids took the place of the larger $Bi_2O_3$ particles [Fig. 3(b)]. Formation of faceted particles in some regions is also apparent. After heat treatment at 825 °C, distinct regions of larger faceted particles, as well as the smaller particles of the size of the original batch, may be seen [Fig. 3(c)]. After heat-treatment at 1000 °C, 5 μm cube-shaped particles formed [Fig. 3(d)].

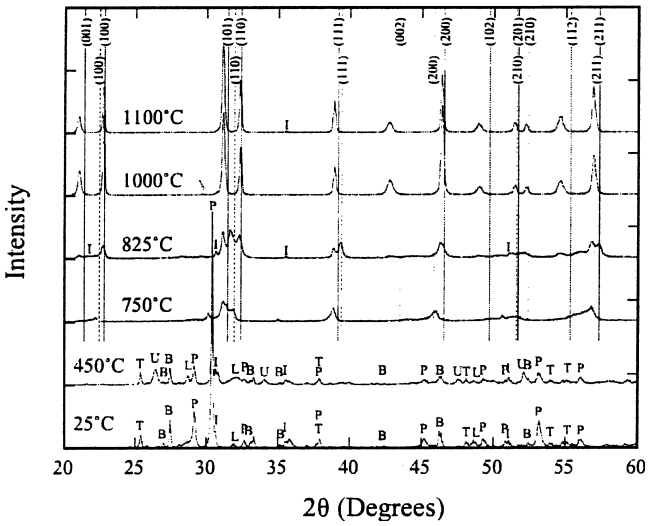


FIG. 1. XRD patterns for $x = 0.15$ heat treated to various temperatures. Symbols have the same meaning as in Table I. Solid lines correspond to ICDD data for $PbTiO_3$ adopting the tetragonal perovskite structure and similarly, dashed lines indicate cubic-structured $PbTiO_3$.

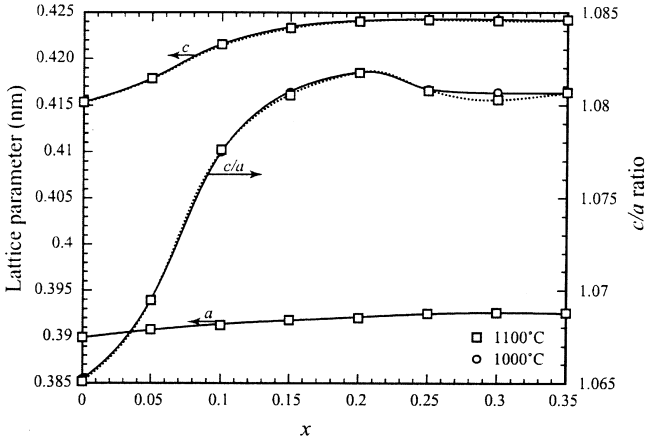


FIG. 2. Change in the lattice parameters $a$, $c$, and their ratio versus composition and temperature.

TABLE I. Phases identified after heat-treatment of compositions to various temperatures. T: $TiO_2$ (anatase, ICDD: 21-1272). B: $Bi_2O_3$ (ICDD: 41-1449). P: PbO (massicot, i.e., yellow lead oxide, ICDD: 38-1477). L: PbO (litharge, ICDD: 05-0561). I: $In_2O_3$ (ICDD: 06-0416). R: $PbTiO_3$, tetragonal perovskite structure (e.g., ICDD: 06-0452). C: cubic $PbTiO_3$ (ICDD: 40-0099). Q: $Pb_3Bi_2O_6$ (ICDD: 45-0657). U: unidentified peaks at 26.4° and 34.2° 2θ. Subscript "*tr*" indicates a trace quantity.

| Temperature | $x = 0.05$ | $x = 0.10$ | $x = 0.15$ | $x = 0.20$ | $x = 0.25$ | $x = 0.30$ | $x = 0.35$ |
|---|---|---|---|---|---|---|---|
| 25 °C | T,B,I,P,L | T,B,I,P,L | T,B,I,P,L | T,B,I,P,L | T,B,I,P,L | T,B,I,P,L | T,B,I,P,L |
| 450 °C | T,B,I,P,L,U | T,B,I,P,L,U | T,B,I,P,L,U | T,I,B,P,L,U | T,B,I,P,L,U | T,B,I,P,L,U | T,B,I,P,L,U |
| 750 °C | C,$R_{tr}$,I | C,$R_{tr}$,I | C,$R_{tr}$ | C,I | C,I | C,I,Q | C,I,Q |
| 825 °C | R | R,$I_{tr}$ | C,R,I | C,$R_{tr}$,I | C,R,I | C,R,I,Q | C,R,I,Q |
| 1000 °C | R,$I_{tr}$ | R,$I_{tr}$ | R | R,$I_{tr}$ | R,I | R,I,Q | R,I,Q |
| 1100 °C | R | R,$I_{tr}$ | R,$I_{tr}$ | R,$I_{tr}$ | R,$I_{tr}$ | R,I,Q | R,I,Q |

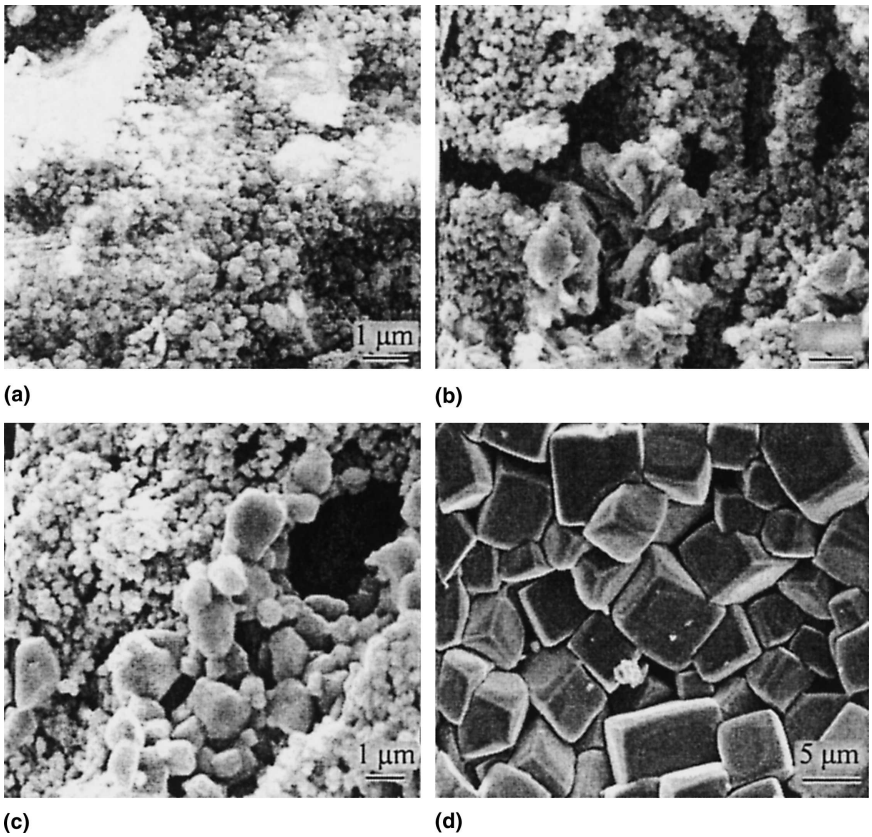


FIG. 3. Secondary electron SEM images: (a) green body compact before heat-treatment ($x = 0.15$); (b) fractured surface of a $x = 0.15$ fired compact soaked at 750 °C for 4 h; (c) fractured surface of a $x = 0.15$ fired compact soaked at 825 °C for 4 h; and (d) fractured surface of a $x = 0.15$ fired compact soaked at 1000 °C for 2 h.

Dimensional densities of microstructures, such as that in Fig. 3(d), were 65% theoretical. Theoretical densities (TD) were calculated based on lattice parameters measured for the various compositions from XRD.

Two-step firing, with an 850 °C pre-calcining step, resulted in more densified microstructures (Fig. 4). Densities of samples with $x = 0.05$ and $x = 0.10$ are not plotted in Fig. 4 since they broke apart after firing. The $x = 0.20$ composition soaked at 1100 °C sintered to 93.0% TD. A typical microstructure after such a two-step firing is shown in Fig. 5(a). After crushing the agglomerated cubes formed by pre-calcining at the higher temperature of 1000 °C, re-pressing and re-firing, an Archimedes density of 94.7% TD was obtained [Fig. 5(b)].

Figure 6 shows DSC traces of samples with various compositions as a function of temperature. Endotherm onsets, interpreted as the Curie temperatures (ferroelectric–paraelectric transformation), increased significantly with $x$ up to $x = 0.15$. Figure 7 shows the DSC-determined Curie temperature overlayed with the XRD-determined $c/a$ ratio as a function of composition; both traces follow a similar trend. A sample for which $x = 0.15$, soaked at 825 °C, which showed both tetragonal and pseudo-cubic-structured (see discussion) perovskite phases, showed two distinct DSC endotherms (Fig. 8, traces $a$ and $b$). The higher temperature endotherm matches with the Curie temperature endotherm for this composition after soaking at 1100 °C (trace $c$). Curie

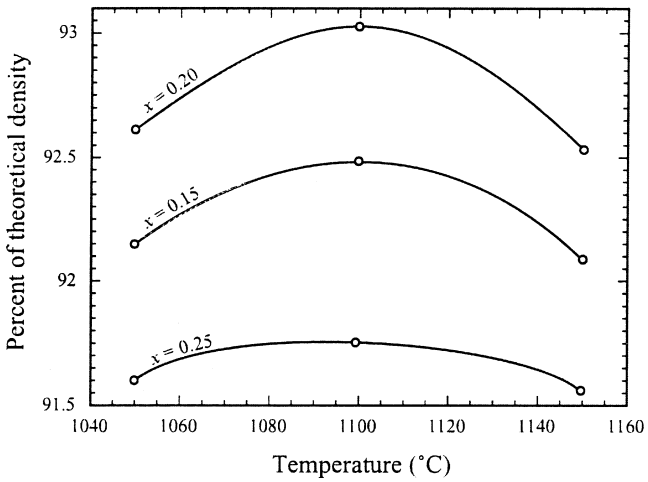


FIG. 4. Archimedes densities, relative to theoretical densities, for various compositions calcined at 850 °C for 4 h, milled, re-pressed, and then soaked at various temperatures for 2 h.

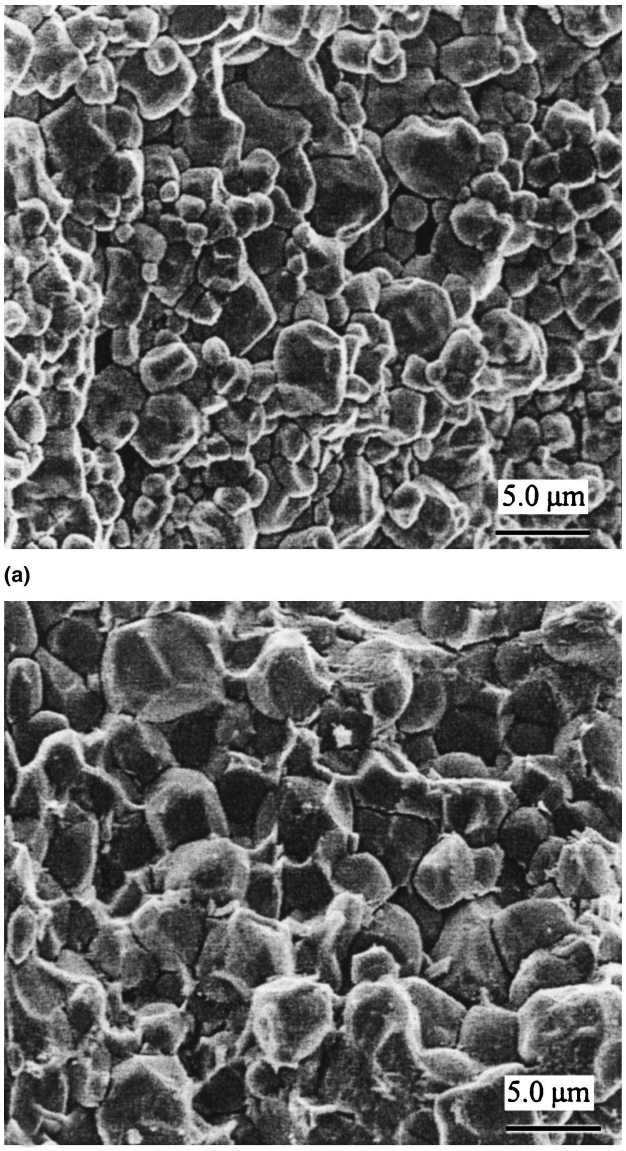


FIG. 5. (a) Fractured surface of a $x = 0.15$ specimen pre-reacted from mixed oxide powders at 850 °C for 4 h, re-milled, dry pressed at 150 MPa, and heat treated at 1100 °C for 2 h; (b) fractured surface of a $x = 0.15$ specimen pre-reacted from mixed oxide powders heat treated at 1000 °C for 4 h, crushed with a mortar and pestle, dry pressed at approximately 150 MPa, and heat treated at 1150 °C for 2 h.

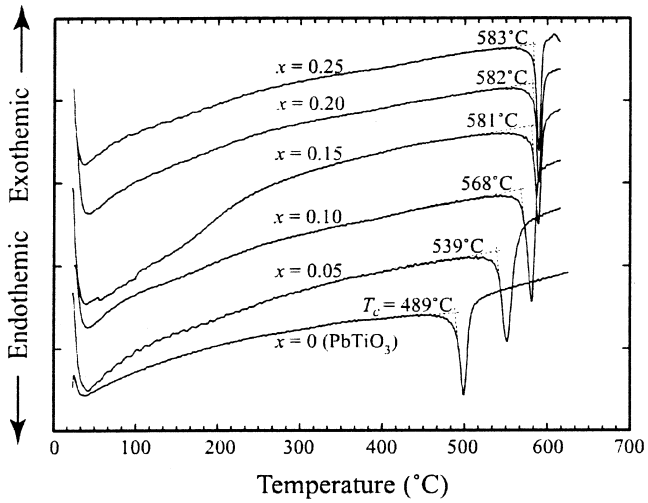


FIG. 6. DSC traces of specimens of various compositions, previously soaked at 1100 °C for 2 h. Scan rate: 8 °C/min.

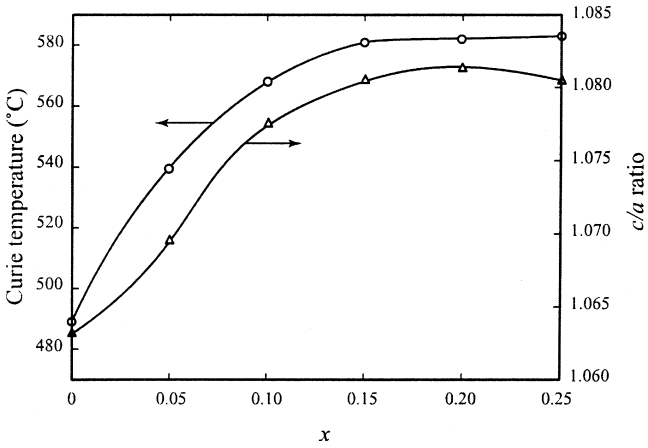


FIG. 7. DSC-determined Curie temperature and XRD-determined *c/a* ratio of samples soaked at 1100 °C for 2 h as a function of composition.

temperatures measured by DSC matched those determined by dielectric permittivity measurements. Dielectric permittivity and loss for an $x = 0.20$ sintered specimen are shown in Fig. 9.

## B. Sol-gel fabrication

DTA traces of heated gels showed partially superimposed exotherms in the range 250–400 °C in nearly the same position for all values of *x*. A smaller exotherm over the range 420–520 °C was apparent for batches of low $x$ ($0.05 \leq x \leq 0.15$), which was not observed for batches with $x = 0.20$ and higher. For all batches, a sharp weight loss was measured over the range 200–300 °C, with a minor residual weight loss measured above 300 °C for $x \leqslant 0.10$. The final weights reached were ~70% of original weight, except for $x = 0.35$ which had its final weight at 79% of its original weight.

Table II shows the XRD-identified phases after heat treatment of sol-gel-prepared $x$BI–$(1 - x)$PT, as a function of soak temperature and composition. For samples soaked in the range 450–600 °C, phase-pure tetragonal perovskite was identified for $x \leqslant 0.10$ and a cubic perovskite phase best-corresponded to XRD peaks for $x \geqslant 0.15$, with $In_2O_3$ identified as a second phase for $x \geqslant 0.30$. XRD results from 600 °C soaks for various compositions are shown in Fig. 10, where both pseudo-cubic and tetragonal structured perovskite diffraction peaks were broadened. XRD patterns for $x = 0.15$ as a function

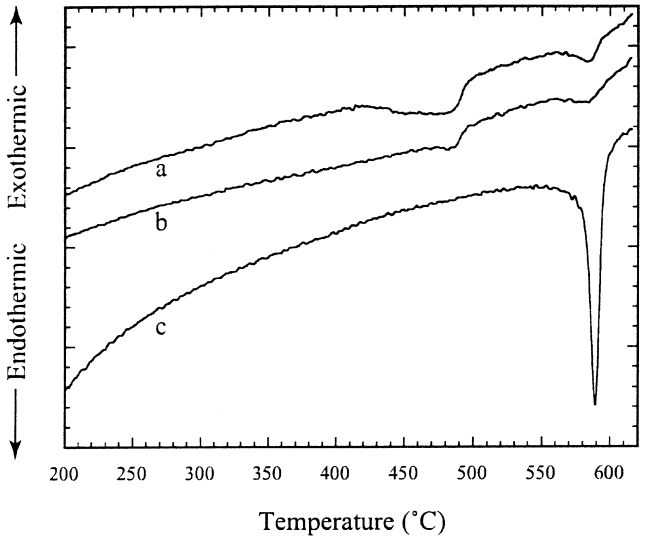


FIG. 8. DSC traces: (a) $x = 0.15$ specimen previously heat treated at 825 °C for 4 h, showing XRD peaks corresponding to both pseudo-cubic and tetragonal perovskite structures, first DSC scan; (b) repeated DSC scan on the same specimen as in (a); and (c) $x = 0.15$ specimen previously heat-treated at 1100 °C for 2 h, showing a tetragonal perovskite structure.

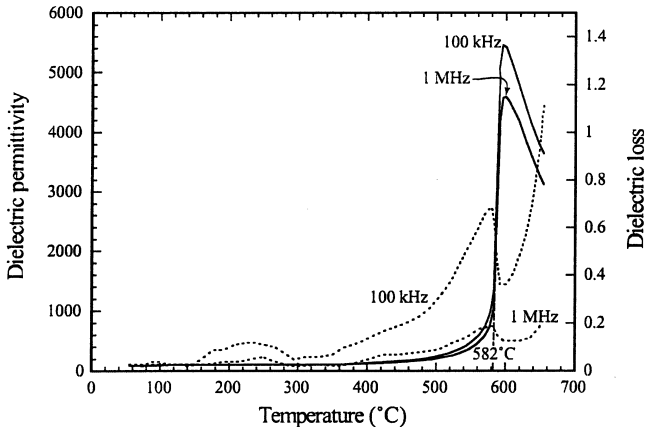


FIG. 9. Dielectric permittivity and loss of a sintered $x = 0.20$ specimen [prior heat-treatment same as in caption for Fig. 5(b)] as a function of temperature evaluated as two frequencies.

of temperature are shown in Fig. 11. After two-step processing, broadened peaks converted to sharp peaks. Lattice parameter calculations on the pseudo-cubic structured perovskite phases ($x \geq 0.15$), i.e., assuming a single lattice parameter for all diffraction peaks, showed inconsistencies. Lattice parameter dilation for the tetragonal perovskite-structured phase formed after two-step heat treatment at 1150 °C as a function of $x$ is shown in Fig. 12.

DSC traces of all compositions showing the broadened pseudo-cubic or tetragonal perovskite structures showed no endotherm corresponding to a Curie temperature transformation. However after two-step heat treatments, similar DSC results to those of mixed oxides were observed.

Figure 13(a) is a TEM micrograph of a $x = 0.05$ sol-gel-prepared powder heat-treated at 600 °C, showing an average particle size of 50 nm. Figure 14 shows the particle sizes of sol-gel processed samples with different $x$ after heat-treatment at various temperatures up to 600 °C, based on XRD peak broadening. For samples soaked at the same temperature, average particle sizes decreased with increasing $x$. For temperatures below 550 °C, average particle size increased slightly with increasing soak temperature.

Figure 13(b) shows the microstructure of a two-step fired sol-gel-prepared sample, showing an average grain size of 5 μm. Table III shows the Archimedes densities of two-step fired sol-gel-prepared samples. These densities were higher than those obtained with mixed oxide powders; the $x = 0.20$ sample reached 98.1% TD.

## IV. DISCUSSION

### A. Mixed oxides

Mixed oxide raw materials reacted between 450 and 750 °C. $Bi_2O_3$ melts at 825 °C but forms eutectic liquids with other batch constituents at lower temperatures; the $Bi_2O_3$–PbO binary system[8] shows a 730 °C eutectic. The $Bi_2O_3$ particles fused, wetting and reacting with the remaining particles, in turn forming a pseudo-cubic perovskite structured phase either at the soaking temperature or during cooling. This phase is referred to as pseudo-cubic since the individual diffraction peaks did not split into peaks corresponding to a tetragonal distortion, yet do not all uniformly fit a single lattice parameter. A noncubic distortion of some form for this phase is also implied by the DSC endotherm (Fig. 8) attributed to that phase, interpreted as a Curie temperature transformation which would only occur in a noncubic phase. Cube-shaped particles of tetragonal perovskite-structured compound then grew out of the liquid phase starting at 750 °C (to a greater extent for lower values of $x$). After heat treatment at 825 °C for $x \leq 0.10$ and after heat treatment at 1000 °C for higher values of $x$, the microstructure had completely transformed to the tetragonal perovskite cubes. For compositions up to $x = 0.25$, virtually phase-pure $x$BI–$(1 - x)$PT formed (i.e., only trace amounts of $In_2O_3$ were detected).

The solubility of Bi and In in the $PbTiO_3$ solid solution for $x \leq 0.25$ is confirmed both by the fact that additional phases of $In_2O_3$ and $Pb_3Bi_2O_6$ were detected only for $x \leq 0.30$, and by the $a$ and $c$ lattice parameters remaining unchanged only over this latter compositional range. The maximum tetragonal distortion, $c/a = 1.082$, was measured for $x = 0.20$, though the vast majority of lattice distortion had occurred by $x = 0.15$ (for pure $PbTiO_3$, $c/a = 1.065$). This is borne out by DSC-measured Curie

TABLE II. Phases detected from sol-gel-processed samples of various compositions, after heated-treating at the indicated temperatures for 6 h (450–600 °C) or in two-step processes, heat-treated at 600 °C for 6 h, crushed, re-pressed, and then heat-treated at 1000 or 1150 °C for 2.5 h. R: tetragonal perovskite $PbTiO_3$ (e.g., ICDD: 06-0452). C: cubic perovskite $PbTiO_3$ (e.g. ICDD: 40-0099). I: $In_2O_3$ (ICDD: 06-0416). Q: $Pb_3Bi_2O_6$ (ICDD: 45-0657). U′: Unidentified peak at 26.8 °C 2θ. —: Broadened peaks which could not be identified. X: Specimen fused.

| Temperature | $x = 0.05$ | $x = 0.10$ | $x = 0.15$ | $x = 0.20$ | $x = 0.25$ | $x = 0.30$ | $x = 0.35$ |
|---|---|---|---|---|---|---|---|
| 450 °C | R | R | C | C | — | — | — |
| 500 °C | R | R | C | C | C | C | C, I |
| 550 °C | R | R | C | C | C | C,I | C,I,U′ |
| 600 °C | R | R | C | C | C | C,I | C,I,U′ |
| 1000 °C | R | R | C,R,I | R,I | R,I | R,I,Q | R,I,Q |
| 1150 °C | R | R | R | $R,I_{tr}$ | R,I | R,I,Q | X |

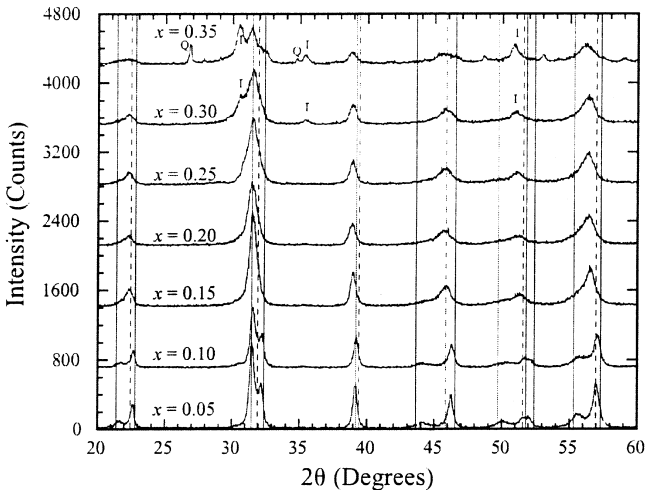


FIG. 10. XRD patterns of sol-gel prepared powders heat treated at 600 °C for 6 h. Dashed lines correspond to cubic $PbTiO_3$ (ICDD: 40-0099) and solid lines correspond to the tetragonal $PbTiO_3$ (ICDD: 06-0452). (I) $In_2O_3$ (ICDD. 06-0416); (Q) $Pb_3Bi_2O_6$ (ICDD: 45-0657).

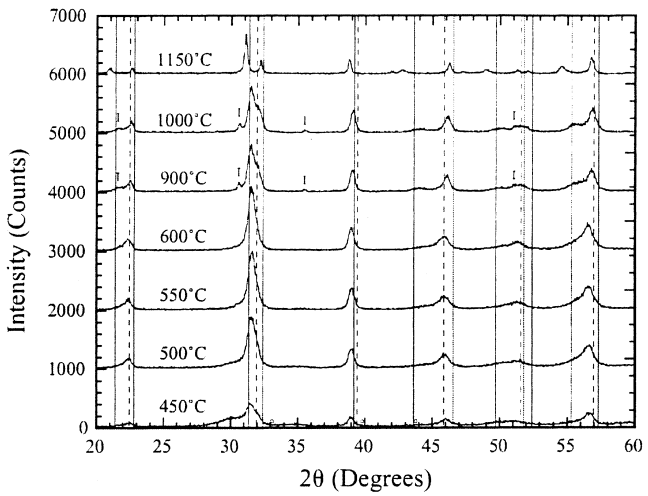


FIG. 11. XRD patterns of sol-gel prepared powders of $x = 0.15$ soaked at various temperatures. Diffraction patterns labeled 900, 1000, and 1150 °C correspond to a two-step heat treatment. Markers and lines are as defined in Fig. 10.

temperatures, which reached a near-saturated value of 581 °C for $x = 0.15$. The DSC-determined Curie temperature for pure $PbTiO_3$ of 489 °C corresponds well to the literature value of 490 °C.[9] DSC and dielectric permittivity measurements of Curie temperature correlate well. In Fig. 9, the sharp peak in permittivity at the Curie temperature is indicative of a first-order phase change, as would be expected from a high level of tetragonality. With increasing temperature leading up to the Curie temperature, the domains were breaking down, and during that process, they moved more easily with the applied field, causing increased loss. At and past the Curie temperature, the decay in loss was from the absence of hysteresis. Losses then increased with temperature because of electron conduction.

The formation of randomly-oriented tetragonal perovskite cubes during the initial heat-treatment did not lend toward the formation of a dense microstructure. Heat treatments at 1100 °C appeared to provide the closest approach (Fig. 4). Below that temperature, inadequate thermal energy was provided for sintering, and above that temperature, the vapor pressure of lead oxide (as

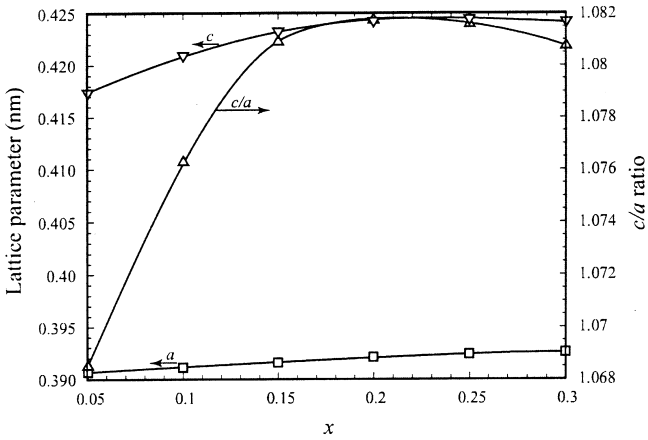


FIG. 12. Change in the lattice parameters $a$ and $c$, and their ratio versus composition for sol-gel prepared specimens soaked at 1150 °C for 2 h.

well as bismuth and indium oxides) became a factor. Upon pulverizing the cube agglomerates, the cubes then assembled tightly upon re-pressing, resulting in a higher density after a second firing. This was especially true if

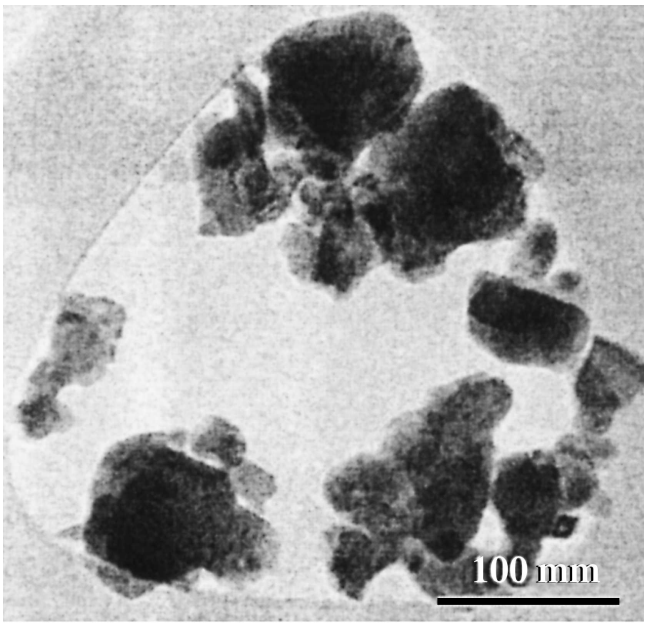


(a)

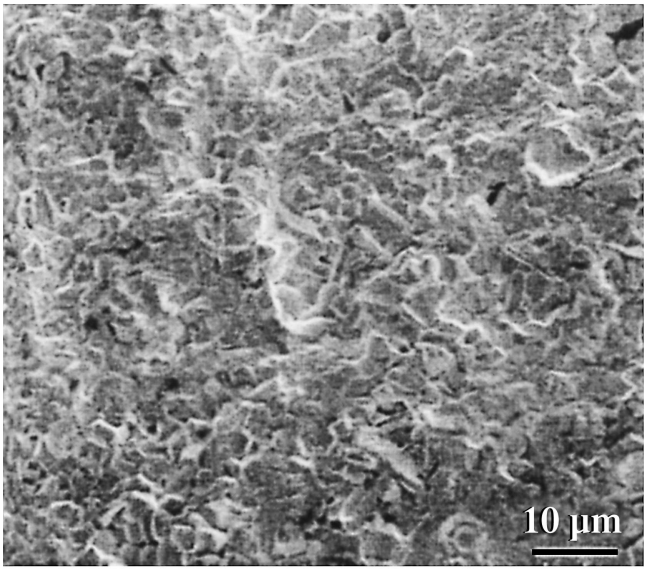


(b)

FIG. 13. (a) TEM micrograph of sol-gel-prepared powder soaked at 600 °C for 6 h and (b) SEM micrographs of fractured surface of a sol-gel-prepared $x = 0.20$ composition, calcined at 600 °C for 6 h, crushed and pressed into a pellet which was soaked at 1150 °C for 2.5 h.

the cubes were fully formed, e.g., after calcining at 1000 °C, in which a fired density of 94.7% of theoretical was obtained from dry-pressed particles with no additives. Use of processing organics to increase green body density should further improve the fired density of the mixed oxides. This and the possibility of textured microstructures via sintering of a pressed assembly of aligned cubes is currently being investigated in our laboratory.

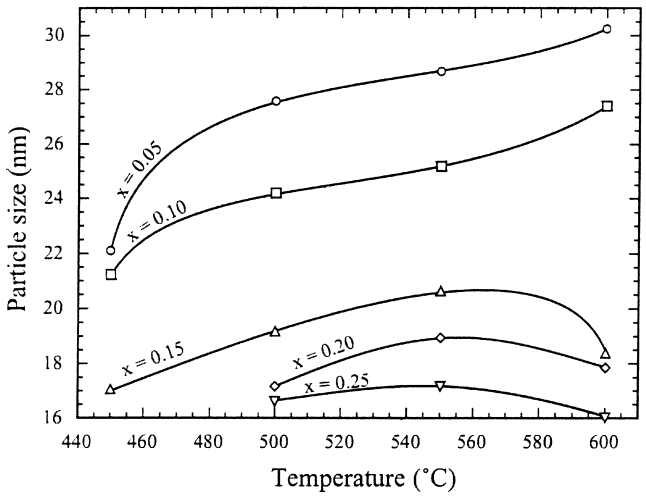


FIG. 14. Particle sizes of the sol-gel-processed samples as a function of composition and soaking temperature.

TABLE III. Archimedes densities (relative to theoretical densities) of sol-gel-prepared samples of various compositions, exposed to the two-step heat treatment described in the caption to Figure 13(b).

| $x$ | % of TD |
|---|---|
| 0.05 | 96.7 |
| 0.10 | 96.2 |
| 0.15 | 97.1 |
| 0.20 | 98.1 |
| 0.25 | 95.9 |

## B. Sol-gel fabrication

Reactions among sol-gel constituents to form a phase-pure perovskite compound occurred as low as 200–300 °C. For $x \leqslant 0.10$, the formed compound was tetragonal, while for higher values of $x$, it was pseudo-cubic. For these compositions, this pseudo-cubic phase converted to tetragonal after two-step heat-treating at or above 1000 °C. After soaking at 1150 °C, not even trace amounts of $In_2O_5$ were detected for compositions of $x \leqslant 0.15$. The extent of $x$, which formed phase-pure perovskite solid solution was the same as for mixed oxides, as was the trend in dilation of $c$ and $a$ lattice parameters.

The average particle size of the sol-gel-prepared calcined particles was substantially smaller than the average size of cubes formed from reaction among mixed oxides, 25 nm compared to 5 μm for mixed oxides. Upon crushing, pressing, and re-firing sol-gel specimens, higher fired densities were obtained for sol-gel-prepared samples (as high as 98.2% TD) as compared to those obtained from calcined mixed oxide particles. Grain sizes for these two-step fired sol-gel samples were 2 orders of magnitude larger than the particles formed after the first heat-treatment step. The mechanism by which this substantial coarsening occurs remains to be established. For both mixed oxide and sol-gel-based fabrication methods,

within the solubility limits observed, a change in perovskite structure via passing through the MPB was not detected.

## V. CONCLUSIONS

The solubility limit of BI in $x$BI–$(1 - x)$PT was $x = 0.25$. Curie temperature and lattice distortion increased rapidly with $x$ up to near-saturation at $x = 0.15$ with a corresponding Curie temperature of 581 °C. In mixed oxide powders, $Bi_2O_3$ particles fused and reacted with the other batch constituents to form liquid phase, from which 5 μm tetragonal perovskite cubes precipitated. Upon two-step firing, densities of 94.7% TD were obtained. Sol-gel fabrication yielded similar results with respect to solubility limit and Curie temperatures. After two-step firing of calcined nano-sized sol-gel powders, tetragonal perovskite microstructures of as high as 98.2% TD were formed.

## REFERENCES

1. B. Jaffe, W.R. Cook, and H. Jaffe: *Piezoelectric Ceramics* (Academic Press, New York, 1971).
2. R.C. Turner, P.A. Fuierer, R.E. Newnham, and T.R. Shrout: Materials for High Temperature Acoustic and Vibration Sensors: A Review. *Appl. Acoustics* **41,** 299 (1994).
3. *Piezoelectric Materials in Devices,* edited by N. Setter (EPFL, Switzerland, 2001).
4. V.M. Goldschmidt: Shrifter Norskevidenskop-Adad. Oslo: Matemot. Natureid Klasse (1926).
5. R.E. Eitel, C.A. Randall, T.R. Shrout, S.E. Park, P. Rehrig, and W. Hackenberger: *Jpn. J. Appl. Phys.* **40,** 5999 (2001).
6. B.D. Cullity: *Elements of X-Ray Diffraction,* 2nd ed. (Addison Wesley, Reading, MA, 1978).
7. J.S. Reed: *Principles of Ceramic Processing,* 2nd ed. (John Wiley and Sons, New York, 1995).
8. E.M. Levin, C.R. Robbins, and H.F. McMurdie: *Phase Diagrams for Ceramists* (American Ceramic Society, Westerville, OH, 1964).
9. Y. Xu: *Ferroelectric Materials and Their Applications* (North-Holland, 1991).